Characterization of chain alignment at buried interfaces using Mueller matrix

spectroscopy

Bryan H. Smith, Renxuan Xie, Wonho Lee, Dipendra Adhikari, Nikolas J. Podraza<sup>2,3</sup> and

Enrique D.  $Gomez^{1,4,5}*$ 

<sup>1</sup>Department of Chemical Engineering, The Pennsylvania State University, University Park, PA

16802

<sup>2</sup>Department of Physics and Astronomy, University of Toledo, Toledo, OH 43606

<sup>3</sup>Wright Center for Photovoltaics Innovation and Commercialization, University of Toledo,

Toledo, OH 43606

<sup>4</sup>Department of Materials Science and Engineering, The Pennsylvania State University, University

Park, PA 16802

<sup>5</sup>Materials Research Institute, The Pennsylvania State University, University Park, PA 16802

\*email: edg12@psu.edu

**Keywords:** spectroscopic ellipsometry; thin films; conjugated polymers; nematic; buried interface

Abstract

The stiffness of conjugated polymers should lead to chain alignment near buried interfaces, even

if the polymer film is nominally amorphous. Although simulations predict that this alignment

layer is approximately 1.5 times the persistence length, chain alignment at buried interfaces of

amorphous polymers has not been experimentally measured. Using Mueller matrix spectroscopy,

we have modeled the optical response of regiorandom poly(3-hexylthiophene-2,5-diyl) (P3HT) in

order to extract the aligned layer thickness. We find that by approximating the optical properties

of the aligned layer as that of regioregular P3HT, the data can be effectively modeled. When the

film is thicker than 150 nm, optical properties are best described with a 4 nm aligned layer, which

is quantitatively consistent with previous predictions.

1

Chain alignment near buried interfaces may improve adhesion, affect transport of small molecules in membranes, and enhance charge mobilities in organic thin-film transistors, 4. Polymers with stiff conformations are predicted to locally align near impenetrable surfaces, such that chain backbones are parallel to the interface. Simulations of bead-spring semiflexible chains predict that the thickness of the backbone alignment layer is approximately 1.5 times the persistence length  $(l_p)$ , even when the polymer is isotropic in the bulk. This uniaxial nematic order (alignment in one axis) near interfaces can also promote the spontaneous formation of biaxial alignment, where nematic coupling leads to domains with locally-aligned chains.

The presence of order at buried interfaces has been detected in semicrystalline polymers using sum-frequency generated spectroscopy<sup>10</sup> and grazing-incidence X-ray diffraction (GIXRD)<sup>4</sup>. Near-edge X-ray absorption spectroscopy, which is sensitive to molecular alignment at surfaces, has demonstrated alignment at air interfaces, or buried interfaces when this surface is exposed through delamination.<sup>11-14</sup> Alignment in films of molecular glasses, where the molecule has a rod-like or disk-like shape, has also been demonstrated through GIXRD, spectroscopic ellipsometry and anisotropic optical absorption.<sup>15-18</sup> Nevertheless, the presence of an aligned buried layer for nominally amorphous and isotropic polymers has not been demonstrated.

Ellipsometry has been used extensively to characterize the optical properties of thin-films composed of conjugated small-molecules or polymers.<sup>14, 19-27</sup> Spectroscopic ellipsometry often relies on evaluating the elements of the diagonal of a 4-complex element Jones matrix collected at a single angle of incidence. Typical ellipsometric spectra are complex and are the ratio of the (1,1) to (2,2) Jones matrix elements. Analyzing only these diagonal Jones matrix elements or their ratio at a single angle of incidence is limited in the ability to fully account for optical anisotropy.

A more general approach to characterize optical anisotropy relies on measuring the 16element Mueller matrix or all 4-complex elements of the Jones matrix. In the absence of depolarization, both representations of the polarization modification of incident light by a sample are sensitive to optical anisotropy (depolarization is not accounted in the Jones matrix representation). The off-diagonal Jones matrix elements or the "upper right" and "lower left" 2 x 2 blocks of the Mueller matrix are non-zero in the presence of in-plane optical anisotropy and zero in its absence. The diagonal Jones matrix elements or the "upper left" and "lower right" 2 x 2 blocks of the Mueller matrix collected at multiple angles of incidence show different measurement angle dependences when out-of-plane optical anisotropy is present or absent. When out-of-plane optical anisotropy and in-plane anisotropy are absent, the only difference in these Jones or Mueller matrix elements arise from the angle of incidence and associated path length difference of the incident beam through the sample layers as the optical response of the layer is isotropic. When out-of-plane optical anisotropy is present, the angle of incidence dependence of these matrix elements depends on both the angular dependent path length difference of the incident beam through the sample layers and sampling of both the in-plane and out-of-plane optical properties of the anisotropic layer. Thus, Mueller matrix spectroscopy is a powerful tool for characterizing the optical response, typically in the form of the complex index of refraction (N = n + ik) spectra, for anisotropic films.<sup>28-30</sup> Optical birefringence, or optically anisotropic materials, can be characterized with Mueller matrix spectroscopy. 31, 32

Here, we demonstrate that Mueller matrix spectroscopy is sensitive to chain alignment near buried interfaces for polymers that are amorphous in the bulk. Inspired by recent simulations of semiflexible polymers that predict the presence of uniaxially aligned layers near buried interfaces, we examine a model conjugated polymer, regionandom poly(3-hexylthiophene-2,5-diyl) (RRa

P3HT), to measure the presence of aligned layers. RRa P3HT is amorphous and isotropic in the bulk,  $^{6,33,34}$  although it has shown dichroism in polarized Fourier-transform infrared spectra from thin films<sup>13</sup>. Mueller matrix spectroscopy of thin-films also shows optical anisotropy, which we describe using a model based on two layers for RRa P3HT films, where optical properties derived from regionegular (RR) P3HT describe an aligned layer near the substrate-film interface. The mean thickness of the aligned layer is  $4.1 \pm 0.5$  nm, in good agreement with the layer thickness predicted from simulations of 4.4 nm.

RRa P3HT was purified using consecutive Soxhlet extractions as previously described.<sup>34,</sup> 35 The molecular weight of RRa P3HT (Aldrich) was measured to be 108 kg/mol using static light scattering (SLS, Figure S1 of the Supplementary Material). Using the radius of gyration obtained from SLS, a persistence length  $l_p$  of  $2.9 \pm 0.4$  nm is obtained, which compares well to predictions from the freely rotating model of 2.8 nm and neutron scattering measurements for RR P3HT that yield 3 nm. 36-38 Films of RRa P3HT and RR P3HT were spun cast on silicon wafers with native oxide using solution concentration to control film thickness. Native oxide thicknesses were obtained prior to spin casting using standard spectroscopic ellipsometry as both silicon and its native oxide are optically isotropic. For RRa P3HT films, multiple spots on multiple samples are measured (Table S1 of the Supplementary Material), whereas one spot was measured for the RR P3HT Films (Table S2 of the Supplementary Material). Films are annealed for 12 hours at 165 °C. Mueller matrix spectra from 210 to 1690 nm are acquired for at least three angles of incidence ranging from 45° to 75° for each film. Dual rotating compensator multichannel ellipsometers (J. A. Woollam Co. model RC-2) were used for data acquisition.<sup>39</sup> The Mueller matrix elements are commonly normalized to the (1, 1) element and represented by Mkl where k indicates the row and l the column of the 4 x 4 matrix. Depolarization is negligible in the measurement samples due to

film and substrate spatial uniformity. Average out-of-plane optical anisotropy is absent as the "upper right" and "lower left" 2 x 2 blocks of the Mueller matrix are zero. In-plane optical anisotropy is measured through simultaneous characterization of the "upper left" and "lower right" 2 x 2 blocks of the Mueller matrix (M12, M21, M22, M33, M34, M43, and M44) collected at multiple angles of incidence. All Mueller matrix elements collected at each angle of incidence are fitted simultaneously in the optical modeling. The ordinary and extra-ordinary optical properties correspond to those obtained in-plane and out-of-plane, respectively.

One of the challenges of spectroscopic ellipsometry and Mueller matrix spectroscopy is the complexity of appropriate models with many adjustable parameters that are often required to properly describe the optical response and structure correctly. We developed our model step wise, with complexity added only as needed. Figure S2 shows schematics of the various models. As a starting point, we consider that each film is represented by only a single isotropic layer as shown in Figure 1a. Data from measurements from each total film thickness are simultaneously fit to derive the Mueller Matrix (MM) spectra with some select elements shown in Figure 1b; Figure S3 shows the optical properties from this model. This isotropic model does not overlap the experimental Mueller matrix elements in P3HT, suggesting further perturbations to this optical model may improve the quality of fit and increase the information gained from the analysis. The appropriateness of a given model compared to others is determined by comparison of the mean square error (MSE) or quality of fit to the experimental data, error on fit parameters, and correlation coefficients between fit parameters. Sample MSE variations for different models are provided in Tables S3 and S4 of the Supplementary Information.

Next, we consider using a single anisotropic layer to fit spectra from each film, thereby allowing for the ordinary and extra-ordinary optical properties to differ but again with a single set of optical properties for all thicknesses (Figure S4a of the Supplementary Material). This model slightly improves the quality of fit. (Figure S4b of the Supplementary Material). The optical properties derived are shown in Figure S5. As expected, the ordinary optical properties are quite similar to the isotropic optical properties.

These two basic models assume that RRa P3HT optical properties are constant with thickness; to investigate this assumption, anisotropic single layer models are developed separately for data obtained from films that vary in total film thickness (Figure S6a of the Supplementary Material). All data collected from films of a given thickness are fit simultaneously. The quality of fit substantially improves, as shown in Figure S6b of the Supplementary Material. We further improve the quality of the fit by including a top layer that is described with a Bruggeman effective medium approximation 0.5 volume fraction polymer optical properties and 0.5 volume fraction air, to account for surface roughness, as shown in Figure 2a.<sup>40</sup>

To quantify how optical properties change with film thickness, the mean 1100 nm birefringence was determined for each set of data as the mean difference between the ordinary refractive index and the extra-ordinary refractive index produced by the model. We use the optical properties at 1100 nm because our materials exhibit no absorption at this wavelength, and the birefringence at 1100 nm is representative of the measured long wavelength portion of the spectrum. Figure 2b shows that birefringence decreases as the film gets thicker. Standard deviations decrease dramatically with thickness, with the 24 nm samples likely being too thin to model with any significant sensitivity to birefringence. Nevertheless, differences between values from thinner films and values for films that are thicker than 150 nm are statistically significant.

Statistical significance was determined using a two-tail p-test that does not assume equal variance. Including or omitting surface roughness in the models does not meaningfully change the results in Figure 2b, as shown in Figure S6c of the Supplementary Material (roughness values are reported in Figure S7).

We also measure the optical anisotropy of RRa P3HT thin films using polarized optical microscopy. Images are taken using crossed and un-crossed polarizers to calculate the birefringence as the ratio of the two images over the same region. Figure S8 of the Supplementary Material corroborates Figure 2b, where the birefringence decreases as a function of film thickness. Assuming weak or modest chain backbone alignment, we would expect that birefringence from polarized microscopy to increase with film thickness, even if the degree of chain alignment is constant with thickness.<sup>41</sup>

Figure 2b and Figure S8 suggest that the decrease in birefringence with film thickness is due to backbone alignment (alignment of chain axes) in the film decreasing as thickness increases. This could be due to the film-substrate interface promoting chain alignment, such that the overall alignment and birefringence in the film decreases as the film gets thicker. To investigate how surface induced chain alignment contributes to the measured birefringence, a second anisotropic layer is added to the model. The optical response of this bottom layer is considered to be the same as those derived from simultaneously modeling regioregular P3HT film measurements with a single anisotropic layer. Regioregular P3HT is semicrystalline and crystals are textured with respect to the substrate, and thereby exhibits much stronger birefringence than amorphous regiorandom P3HT.<sup>31, 32</sup> It was found that the two-layer models are not sensitive enough to independently derive physically realistic optical properties for the bottom layer, necessitating this assumption. The derived RR P3HT optical properties are shown in Figure S9.

Using the RR P3HT properties for the bottom layer, two-layer models with an anisotropic top layer are developed separately for each set of data for a given total film thickness (Figure S10a of the Supplementary Material). Figure S10b shows a slight quality of fit improvement, and Table S3 shows how the calculated MSE over the absorbing region for the 155 nm samples decreases with the refined models. Examination of the mean 1100 nm birefringence in the top layer when roughness is accounted for (Figure S11b) reveals a similar result to those reported in Figure 2, where the thickest two sets of samples exhibit less birefringence than the thinner sets. Roughness values for this model are plotted in Figure S11c. Again, the removal of surface roughness from the model does not substantially change the results as shown in Figure S12.

The two-layer anisotropic model with roughness shown in Figure 3a converged on a non-zero bottom layer thickness for several data sets as shown in Figure 3b. When roughness is removed from the model, the fitting results are essentially unchanged as shown in Figure S12c. Thin films show a nearly negligible strongly-anisotropic bottom layer, but, as shown in Figure S11b of the Supplementary Material, thinner films also show stronger birefringence in the weakly anisotropic (top) layer. We thus hypothesize that thin films are aligned throughout the film thickness, obviating the need for two distinct layers to describe the data. Furthermore, simulations show that the uniaxial alignment induced by the presence of an impenetrable surface can lead to biaxial liquid crystalline order in thin films of stiff polymers, even when the polymer is isotropic in the bulk<sup>3, 9</sup>. Perhaps when films are thin, the alignment induced by the bottom surface leads to the spontaneous formation of a liquid crystalline phase such that order persists throughout the film thickness.

In contrast, films that are 155 nm and 230 nm thick have a bottom layer that is strongly anisotropic and is about 4 nm thick. We attribute this anisotropy to chain alignment near the

bottom surface, with an aligned layer of  $4.1 \pm 0.5$  nm based on the average from the thickest two films shown in Figure 3b. Simulations predict an aligned (uniaxial nematic) layer to an extent of approximately  $1.5 l_p$ , or 4.4 nm or 4.5 nm using either our measured persistence length 2.9 nm (Figure S1) or reported values of 3 nm.<sup>37</sup> This is in close agreement with the thickness of the strongly anisotropic layer of thick RRa P3HT films obtained from modeling of Mueller matrix spectra (Figure 3b).

The inclusion of the aligned bottom layer lowers the MSE in all 155 nm and 230 nm thick sample models. For the 155 nm samples, MSE decreases between 9.8% and 1.2% depending on the dataset. The mean decrease is 5.4% with a standard deviation of 3.2%. For the 230 nm samples, MSE decreases between 1.4% and 0.8% depending on the dataset. The mean decrease is 1.1% with a standard deviation of 0.3%. The MSE decrease supports the inclusion of an aligned layer in the model. Table S4 summarizes how the mean birefringence, interface layer thickness, and MSE change between one and two-layer anisotropic models for the 155 nm films. Parameter uniqueness fits (Figure S13 of the Supplementary Material) performed for the bottom layer thickness in the 155 nm and 230 nm samples show that the models do exhibit sensitivity to the interface thickness, as the fits clearly reach a minimum weighted MSE. When considered with the overall MSE decrease for the two-layer fits, this provides strong evidence that the optically detected aligned layers near the buried interface are meaningful.

There is no meaningful MSE difference between models with and without surface roughness. Nevertheless, films are not expected to be perfectly smooth, and the inclusion of roughness eliminates the possibility that the model is falsely assigning optical response from roughness to the aligned layer. Accounting for surface roughness only adds one degree of freedom to the model.

The correlation coefficients between the top and bottom layer thickness in the two-layer models are greater than 0.99, which indicate that the models are more sensitive to the overall thickness of the sample than to the thickness of the bottom layer alone. Correlation is a consequence of the data analysis being an indirect process and is not unexpected when one parameter has a disproportionate impact on the total optical response of the film. In this case, the total thickness of the film has a larger effect on optical response than the much thinner aligned layer.

A two-layer model with an isotropic top layer and a bottom layer represented again by RR P3HT optical properties is fit to each dataset to see if the anisotropic top layer assumption is critical to the aligned layer thickness results (Figure 14a of the Supplementary Material). As in the model with two anisotropic layers, the top layer optical response and the thickness of both layers are allowed to vary while the bottom anisotropic layer is fixed with the derived RR P3HT optical properties. Figure S14b shows the bottom layer thicknesses using this model for each total film thickness. The thinnest four samples now exhibit a bottom layer ranging from approximately 0.4 nm to 1.4 nm and the thicker 154 nm and 230 nm samples are still found to have significantly thicker bottom layers, which is consistent with the two-layer anisotropic results. Nevertheless, MSE values for fits to two layers with an isotropic top layer are consistently higher than the two-layer anisotropic model and therefore the isotropic top layer model is considered to less precisely fit the data. Another possibility is that an aligned top layer exists, although it appears that the presence of an aligned bottom layer is dominating optical properties, potentially precluding our ability to identify such a layer.

The effect of thermally annealing the films is examined using the two-layer anisotropic model by comparing as-cast films with annealed films. The anneal decreases bulk birefringence

in both 35 nm and 150 nm films while also decreasing the aligned interface layer from around 6 nm to 4.5 nm in the 150 nm films. These results are summarized in Table S5. The spin coating process and conditions likely induces order on the film morphology as has been observed in other polymer systems. Therefore, the thermal anneal allow chains to relax slightly from a state established by spin-casting conditions, although it is clear that a model with a bottom aligned layer best fit the data of films that are not annealed.

In conclusion, RRa P3HT films of various total thickness have been prepared and studied with Mueller matrix spectroscopy in order to characterize predicted alignment at the buried substrate interface. Several models are developed to analyze the data and are compared. A twolayer model in which the top layer is anisotropic and the bottom layer has the same anisotropic optical properties as regioregular P3HT is found to best fit the data. In this model, the thickest samples have a mean bottom layer thickness of 4.4 nm and 3.8 nm respectively, whereas thinner samples are aligned throughout the entire film. Thus, these results provide experimental evidence for the prediction of surface-induced alignment in conjugated polymer films, including the possibility of a 4.5 nm aligned layer in amorphous P3HT films.<sup>3</sup> Such chain alignment could enhance in-plane charge transport by orders of magnitude, 44 such that we predict RRa P3HT transistors would exhibit even lower mobilities than reported (ca. 10<sup>-6</sup> cm<sup>2</sup>/Vs),<sup>35, 45</sup> if fully isotropic films could be made (despite the presence of an aligned layer in RRa P3HT, mobilities of devices based on RR P3HT mobilities are significantly higher, around 10<sup>-1</sup> cm<sup>2</sup>/Vs<sup>46</sup>, likely due to significantly higher degree of  $\pi$ - $\pi$  stacking). Our analysis of the optical anisotropy suggests that in thinner films, the interface induces moderate order throughout the film, whereas above a critical thickness, the interface induces strong alignment only a few nanometers into the bulk of the film.

The quality of the fit to Muller matrix spectra using models with chain backbone alignment

at the buried interface in thicker films is found to be relatively insensitive to minor procedural

changes including removal of surface roughness from the model, modeling the bulk of the RRa

P3HT as isotropic rather than anisotropic, and not thermally annealing the films before

measurement. Significant decreases in MSE justify the inclusion of an aligned buried interface

layer in the model as well as treating the bulk of the RRa P3HT as having anisotropic properties

that change with thickness. The parameter uniqueness tests and correlation coefficients are

consistent with a physically meaningful model. The modeling strategy outlined here is robust

enough to apply to a variety of polymer systems for the further study of semiflexible polymer

interface alignment and its effect on material properties.

**Supplementary material** 

Supplementary material includes:

Materials and methods, thicknesses of films used in this study, static light scattering,

polarized optical microscopy, optical models, and spectroscopic ellipsometry results

(PDF).

Acknowledgements

Funding from the National Science Foundation through Award DMREF-1629006 and DMREF-

1921854 is gratefully acknowledged. The authors thank Prof. Tom Jackson for use of a

spectroscopic ellipsometer.

**Table of contents graphic:** Figure 3c

12

## References

- 1. M. Leolukman and S.H. Kim: Effect of Rubbing-Induced Polymer Chain Alignment on Adhesion and Friction of Glassy Polystyrene Surfaces. *Langmuir* **21**, 682 (2005).
- 2. J. Li, J.K. Park, R.B. Moore and L.A. Madsen: Linear coupling of alignment with transport in a polymer electrolyte membrane. *Nat. Mater.* **10**, 507 (2011).
- 3. W. Zhang, E.D. Gomez and S.T. Milner: Surface-Induced Chain Alignment of Semiflexible Polymers. *Macromolecules* **49**, 963 (2016).
- 4. R. Joseph Kline, M.D. McGehee and M.F. Toney: Highly oriented crystals at the buried interface in polythiophene thin-film transistors. *Nat. Mater.* **5**, 222 (2006).
- 5. J.Z.Y. Chen and D.E. Sullivan: Free energy of a wormlike polymer chain confined in a slit: crossover between two scaling regimes. *Macromolecules* **39**, 7769 (2006).
- 6. J.Z.Y. Chen, D.E. Sullivan and X. Yuan: Surface-induced liquid crystal transitions of wormlike polymers confined in a narrow slit. A mean-field theory. *Macromolecules* **40**, 1187 (2007).
- 7. V.A. Ivanov, A.S. Rodionova, E.A. An, J.A. Martemyanova, M.R. Stukan, M. Müller, W. Paul and K. Binder: Orientational ordering transitions of semiflexible polymers in thin films: A Monte Carlo simulation. *Physical Review E* **84**, 041810 (2011).
- 8. D.C. Morse and G.H. Fredrickson: Semiflexible polymers near interfaces. *Physical review letters* **73**, 3235 (1994).
- 9. W. Zhang, E.D. Gomez and S.T. Milner: Using surface-induced ordering to probe the isotropic-to-nematic transition for semiflexible polymers. *Soft Matter* **12**, 6141 (2016).
- 10. M. Xiao, J. Jasensky, X. Zhang, Y. Li, C. Pichan, X. Lu and Z. Chen: Influence of the side chain and substrate on polythiophene thin film surface, bulk, and buried interfacial structures. *Phys. Chem. Chem. Phys.* **18**, 22089 (2016).
- 11. D.M. DeLongchamp, E.K. Lin and D.A. Fischer: Organic semiconductor structure and chemistry from near-edge X-ray absorption fine structure (NEXAFS) spectroscopy, in Optics and Photonics 2005 (SPIE2005), p. 59400A.
- 12. H. Wang, E.D. Gomez, Z. Guan, C. Jaye, M.F. Toney, D.A. Fischer, A. Kahn and Y.-L. Loo: Tuning Contact Recombination and Open-Circuit Voltage in Polymer Solar Cells via Self-Assembled Monolayer Adsorption at the Organic–Metal Oxide Interface. *J. Phys. Chem. C* 117, 20474 (2013).

- 13. M.C. Gurau, D.M. Delongchamp, B.M. Vogel, E.K. Lin, D.A. Fischer, S. Sambasivan and L.J. Richter: Measuring Molecular Order in Poly(3-alkylthiophene) Thin Films with Polarizing Spectroscopies. *Langmuir* **23**, 834 (2007).
- 14. D.S. Germack, C.K. Chan, R.J. Kline, D.A. Fischer, D.J. Gundlach, M.F. Toney, L.J. Richter and D.M. DeLongchamp: Interfacial Segregation in Polymer/Fullerene Blend Films for Photovoltaic Devices. *Macromolecules* **43**, 3828 (2010).
- A. Gujral, J. Gómez, S. Ruan, M.F. Toney, H. Bock, L. Yu and M.D. Ediger: Vapor-Deposited Glasses with Long-Range Columnar Liquid Crystalline Order. *Chem. Mater.* 29, 9110 (2017).
- 16. S.S. Dalal, D.M. Walters, I. Lyubimov, J.J. de Pablo and M.D. Ediger: Tunable molecular orientation and elevated thermal stability of vapor-deposited organic semiconductors. *Proceedings of the National Academy of Sciences* **112**, 4227 (2015).
- 17. A. Gujral, K.A. O'Hara, M.F. Toney, M.L. Chabinyc and M.D. Ediger: Structural Characterization of Vapor-Deposited Glasses of an Organic Hole Transport Material with X-ray Scattering. *Chem. Mater.* **27**, 3341 (2015).
- 18. D.M. Walters, L. Antony, J.J. de Pablo and M.D. Ediger: Influence of Molecular Shape on the Thermal Stability and Molecular Orientation of Vapor-Deposited Organic Semiconductors. *The Journal of Physical Chemistry Letters* **8**, 3380 (2017).
- 19. M. Campoy-Quiles, T. Ferenczi, T. Agostinelli, P.G. Etchegoin, Y. Kim, T.D. Anthopoulos, P.N. Stavrinou, D.D.C. Bradley and J. Nelson: Morphology evolution via self-organization and lateral and vertical diffusion in polymer: fullerene solar cell blends. *Nature materials* 7, 158 (2008).
- 20. D.M. DeLongchamp, R.J. Kline, D.A. Fischer, L.J. Richter and M.F. Toney: Molecular characterization of organic electronic films. *Advanced Materials* **23**, 319 (2011).
- 21. D.M. DeLongchamp, R.J. Kline, E.K. Lin, D.A. Fischer, L.J. Richter, L.A. Lucas, M. Heeney, I. McCulloch and J.E. Northrup: High carrier mobility polythiophene thin films: structure determination by experiment and theory. *Advanced Materials* **19**, 833 (2007).
- 22. C.M. Ramsdale and N.C. Greenham: Ellipsometric Determination of Anisotropic Optical Constants in Electroluminescent Conjugated Polymers. *Adv. Mater.* **14**, 212 (2002).
- 23. I. McCulloch, M. Heeney, M.L. Chabinyc, D. DeLongchamp, R.J. Kline, M. Cölle, W. Duffy, D. Fischer, D. Gundlach and B. Hamadani: Semiconducting thienothiophene

- copolymers: design, synthesis, morphology, and performance in thin-film organic transistors. *Adv. Mater.* **21**, 1091 (2009).
- T. Ameri, G. Dennler, C. Waldauf, P. Denk, K. Forberich, M.C. Scharber, C.J. Brabec and K. Hingerl: Realization, characterization, and optical modeling of inverted bulkheterojunction organic solar cells. *J. Appl. Phys.* 103, 084506 (2008).
- 25. G.F. Burkhard, E.T. Hoke and M.D. McGehee: Accounting for Interference, Scattering, and Electrode Absorption to Make Accurate Internal Quantum Efficiency Measurements in Organic and Other Thin Solar Cells. *Adv. Mater.* **22**, 3293 (2010).
- 26. C.-Q. Mariano, A.M. Isabel, B.D.D. C. and R.L. J.: Advanced Ellipsometric Characterization of Conjugated Polymer Films. *Adv. Funct. Mater.* **24**, 2116 (2014).
- 27. C. Müller, L.M. Andersson, O. Peña-Rodríguez, M. Garriga, O. Inganäs and M. Campoy-Quiles: Determination of Thermal Transition Depth Profiles in Polymer Semiconductor Films with Ellipsometry. *Macromolecules* **46**, 7325 (2013).
- 28. E. Garcia-Caurel, A. De Martino, J.-P. Gaston and L. Yan: Application of spectroscopic ellipsometry and Mueller ellipsometry to optical characterization. *Applied spectroscopy* **67**, 1 (2013).
- 29. M. Campoy-Quiles, P.G. Etchegoin and D.D.C. Bradley: On the optical anisotropy of conjugated polymer thin films. *Phys. Rev. B* **72**, 045209 (2005).
- 30. A. Laskarakis, S. Logothetidis, E. Pavlopoulou and M. Gioti: Mueller matrix spectroscopic ellipsometry: formulation and application. *Thin Solid Films* **455**, 43 (2004).
- 31. E.M. Arruda and P.A. Przybylo: An investigation into the three-dimensional stress-birefringence-strain relationship in elastomers. *Polymer Engineering & Science* **35**, 395 (1995).
- 32. B.A. Beiermann, S.L.B. Kramer, P.A. May, J.S. Moore, S.R. White and N.R. Sottos: The Effect of Polymer Chain Alignment and Relaxation on Force-Induced Chemical Reactions in an Elastomer. *Adv. Funct. Mater.* **24**, 1529 (2014).
- 33. S. Hugger, R. Thomann, T. Heinzel and T. Thurn-Albrecht: Semicrystalline morphology in thin films of poly (3-hexylthiophene). *Colloid and Polymer Science* **282**, 932 (2004).
- 34. R. Xie, Y. Lee, M.P. Aplan, N.J. Caggiano, C. Müller, R.H. Colby and E.D. Gomez: Glass Transition Temperature of Conjugated Polymers by Oscillatory Shear Rheometry. *Macromolecules* **50**, 5146 (2017).

- 35. K. Vakhshouri, D.R. Kozub, C. Wang, A. Salleo and E.D. Gomez: Effect of Miscibility and Percolation on Electron Transport in Amorphous Poly(3-Hexylthiophene)/Phenyl-C61-Butyric Acid Methyl Ester Blends. *Physical Review Letters* **108**, 026601 (2012).
- 36. B. Kuei and E.D. Gomez: Chain conformations and phase behavior of conjugated polymers. *Soft Matter* **13**, 49 (2017).
- 37. B. McCulloch, V. Ho, M. Hoarfrost, C. Stanley, C. Do, W.T. Heller and R.A. Segalman: Polymer Chain Shape of Poly(3-alkylthiophenes) in Solution Using Small-Angle Neutron Scattering. *Macromolecules* **46**, 1899 (2013).
- 38. W. Zhang, E.D. Gomez and S.T. Milner: Predicting Chain Dimensions of Semiflexible Polymers from Dihedral Potentials. *Macromolecules* **47**, 6453 (2014).
- 39. C. Chen, I. An, G.M. Ferreira, N.J. Podraza, J.A. Zapien and R.W. Collins: Multichannel Mueller matrix ellipsometer based on the dual rotating compensator principle. *Thin Solid Films* **455**, 14 (2004).
- 40. H. Fujiwara, J. Koh, P.I. Rovira and R.W. Collins: Assessment of effective-medium theories in the analysis of nucleation and microscopic surface roughness evolution for semiconductor thin films. *Phys. Rev. B* **61**, 10832 (2000).
- 41. J.D. Wilbur, E.D. Gomez, M.W. Ellsworth, B.A. Garetz and N.P. Balsara: Thermoreversible Changes in Aligned and Cross-Linked Block Copolymer Melts Studied by Two Color Depolarized Light Scattering. *Macromolecules* **45**, 7590 (2012).
- 42. J.Y. Na, B. Kang, D.H. Sin, K. Cho and Y.D. Park: Understanding solidification of polythiophene thin films during spin-coating: effects of spin-coating time and processing additives. *Sci. Rep.* **5**, 13288 (2015).
- 43. J.-F. Chang, B. Sun, D.W. Breiby, M.M. Nielsen, T.I. Sölling, M. Giles, I. McCulloch and H. Sirringhaus: Enhanced mobility of poly (3-hexylthiophene) transistors by spin-coating from high-boiling-point solvents. *Chem. Mater.* **16**, 4772 (2004).
- 44. W. Zhang, S.T. Milner and E.D. Gomez: Nematic Order Imposes Molecular Weight Effect on Charge Transport in Conjugated Polymers. *ACS Central Science* **4**, 413 (2018).
- 45. C. Wang, J. Rivnay, S. Himmelberger, K. Vakhshouri, M.F. Toney, E.D. Gomez and A. Salleo: Ultrathin Body Poly(3-hexylthiophene) Transistors with Improved Short-Channel Performance. *ACS Applied Materials & Interfaces* **5**, 2342 (2013).

46. B.H. Smith, M.B. Clark, H. Kuang, C. Grieco, A.V. Larsen, C. Zhu, C. Wang, A. Hexemer, J.B. Asbury, M.J. Janik and E.D. Gomez: Controlling Polymorphism in Poly(3-Hexylthiophene) through Addition of Ferrocene for Enhanced Charge Mobilities in Thin-Film Transistors. *Adv. Funct. Mater.* 25, 542 (2015).

## **Figures**

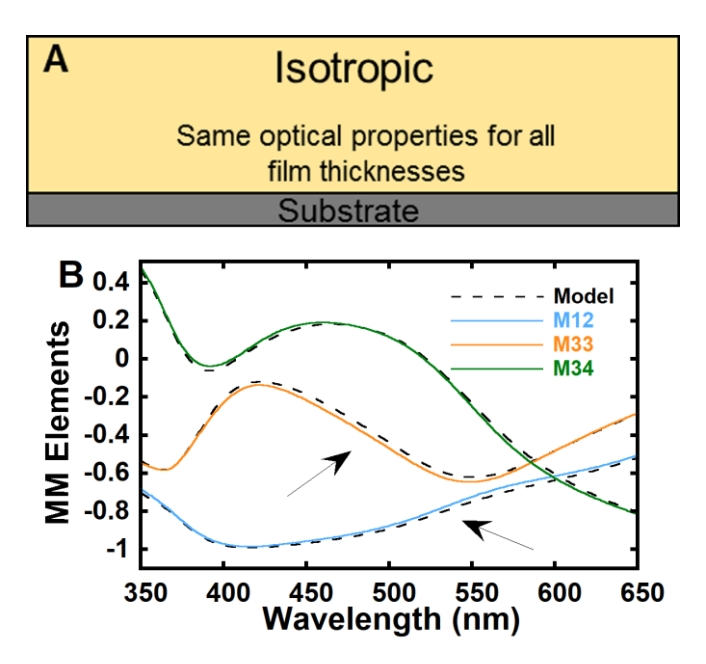


**Figure 1.** (A) Schematic of model used to fit Mueller matrix spectra. RRa P3HT is assumed to have isotropic optical properties that do not vary with film thickness in this analysis. (B) Selected normalized Mueller matrix elements (Mkl, k indicating row and l indicating column) for a 155 nm thick RRa P3HT film at  $60^{\circ}$  incident angle in the 350-650 nm range (solid lines). A one-layer model shown as dashed lines was derived from fitting data in the 210-1690 nm wavelength range for a variety of film thicknesses (24-230 nm) with the same optical properties. Arrows highlight that the fit is not optimal in the 400-600 nm range for M12 and M33.

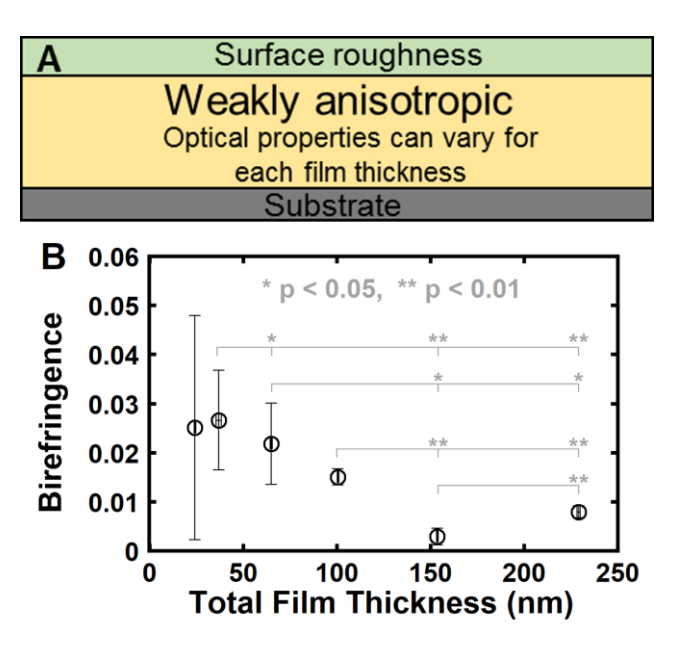


**Figure 2.** (A) Schematic of model used to fit Mueller matrix spectra. Model includes surface roughness and treats RRa P3HT as having weakly anisotropic optical properties that can vary for each film thickness. (B) Mean 1100 nm birefringence shown with standard deviation for regiorandom P3HT films of various thickness as determined using a single layer anisotropic ellipsometry model that accounts for surface roughness. The thickest two sets of samples show statistically significantly reduced birefringence as compared to thinner sets of samples.

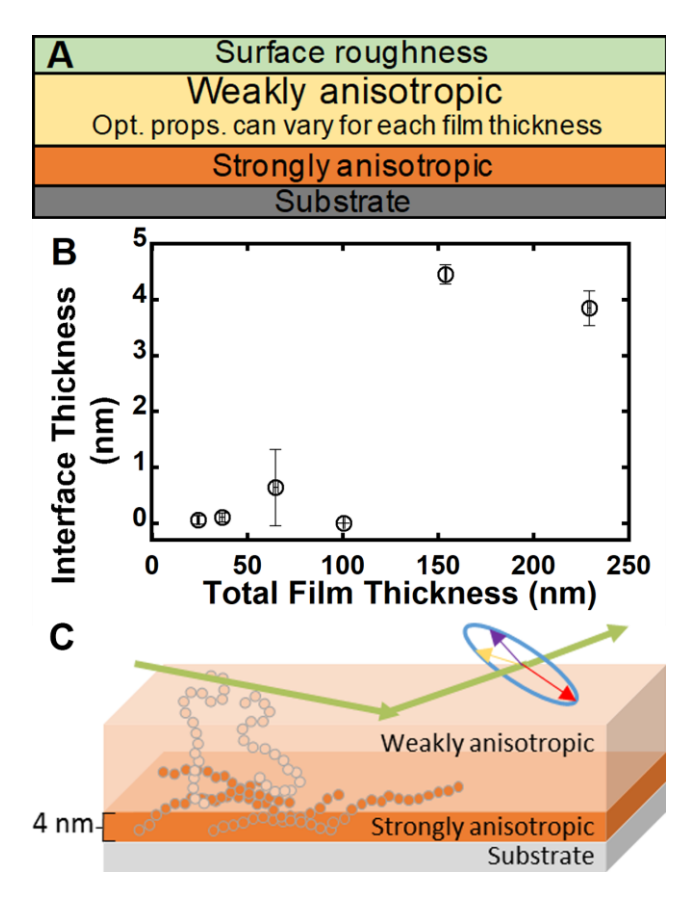


**Figure 3.** (A) Schematic of model used to fit Mueller matrix spectra. Model includes surface roughness and treats RRa P3HT as having weakly anisotropic optical properties that can vary for each film thickness with two distinct layers. Bottom layer near the buried interface has strongly anisotropic properties that are the same for each film thickness and were derived from RR P3HT. (B) Thickness of bottom layer (aligned layer) with standard deviation for regionandom P3HT films of various thickness. The thickest two sets of samples have an aligned layer thickness of about 4 nm, in good agreement with predictions.<sup>3</sup> (C) Schematic of chain alignment with respect to our two layer model derived from Mueller matrix spectroscopy.